

Topological Phase Transition in the Hofstadter-Hubbard Model

Lei Wang¹, Hsiang-Hsuan Hung² and Matthias Troyer¹

¹Theoretische Physik, ETH Zurich, 8093 Zurich, Switzerland and

²Department of Physics, University of Texas at Austin, Austin, Texas 78712, USA

We study the interplay between topological and conventional long range order of attractive fermions in a time reversal symmetric Hofstadter lattice using quantum Monte Carlo simulations, focussing on the case of one-third flux quantum per plaquette. At half-filling, the system is unstable towards s-wave pairing and charge-density-wave order at infinitesimally small interactions. At one-third-filling, the noninteracting system is a topological insulator, and a nonzero critical interaction strength is needed to drive a transition from the quantum spin Hall insulator to a superfluid. We probe the topological signature of the phase transition by threading a magnetic flux through a cylinder and observe quantized topological charge pumping.

PACS numbers: 74.20.-z, 71.27.+a, 03.65.Vf, 73.43.-f

The Hofstadter model [1], which describes electron moving in a 2D lattice subject to a uniform magnetic field, shows an intriguing interplay between band structure and magnetic field giving rise to a fractal energy spectrum and integer quantum Hall states [2, 3]. This model has recently been realized in graphene superlattices [4–6] and ultracold atoms in optical lattices [7, 8]. The latter cold atom experiments, in particular, have realized the Hofstadter model for *two* spin components using *opposite* magnetic fluxes [7, 9]. This system conserves time-reversal-symmetry (TRS) and, when loading fermions into the optical lattice, is a natural realization of the quantum spin Hall (QSH) effect [10, 11] thus connecting the Hofstadter to the active field of topological insulators (TI) [12, 13]. Being a topological insulating state in 2D, the QSH state is one of the first topologically insulating states observed in nature [10, 11, 14]. Tunable local interactions in cold atom experiments allow to address the interesting interplay of interaction effects and the band topology. The problem has been studied in various models such as the Kane-Mele Hubbard model [15–20], the interacting Haldane model [21–23] and the interacting Bernevig-Hughes-Zhang model [24, 25], see [26] for a recent review.

There are, in general, two difficulties when studying interacting effect in topological insulators: the lack of unbiased numerical methods and the difficulty of direct quantification of the topological property of an interacting system. In this Letter we report on a large-scale quantum Monte Carlo (QMC) study of the attractive Hofstadter-Hubbard model, where we overcome both these problems. The sign problem [27, 28] is absent due to the time reversal symmetry of our model. We can thus map out the ground state phase diagram and study the quantum phase transition from a QSH state to a superfluid upon increasing a local attraction between the two spin species. To directly diagnose the topological nature of the correlated TI, we apply Laughlin’s flux insertion technique [29] and observe an induced topological charge pumping effect [30, 31]. These results provide direct evidence for a

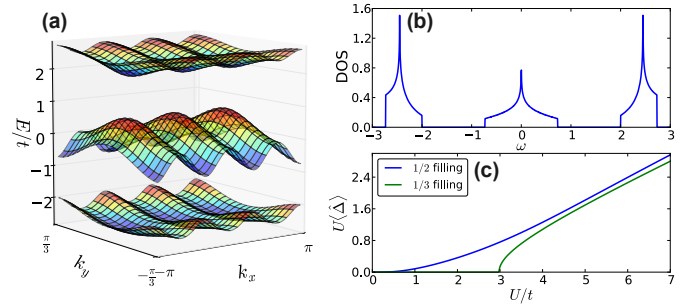


Figure 1: (a) Band structure and (b) density of states of the noninteracting Hofstadter model with $\phi = 1/3$. (c) Mean field result of the superconducting order parameter as a function of attractive interaction strength at 1/2 and 1/3 fillings.

QSH state in an interacting system and a quantum phase transition to a topologically trivial superconductor.

The Model – The Hamiltonian of the time reversal symmetric Hofstadter-Hubbard model reads [32],

$$\begin{aligned}\hat{H} &= \hat{K} + \hat{V}, \\ \hat{K} &= -t \sum_{\mathbf{r}, \sigma} e^{i\sigma 2\pi y_{\mathbf{r}} \phi} \hat{c}_{\mathbf{r}+\hat{\mathbf{x}}\sigma}^\dagger \hat{c}_{\mathbf{r}\sigma} + \hat{c}_{\mathbf{r}+\hat{\mathbf{y}}\sigma}^\dagger \hat{c}_{\mathbf{r}\sigma} + h.c., \\ \hat{V} &= -U \sum_{\mathbf{r}} (\hat{n}_{\mathbf{r}\uparrow} - \frac{1}{2})(\hat{n}_{\mathbf{r}\downarrow} - \frac{1}{2}),\end{aligned}\quad (1)$$

where the operator $\hat{c}_{\mathbf{r}\sigma}$ annihilates a fermion of spin $\sigma = \pm 1$ (corresponding to spin \uparrow and \downarrow fermions). at site $\mathbf{r} = (x_{\mathbf{r}}, y_{\mathbf{r}})$. The phase factor $e^{i\sigma 2\pi y_{\mathbf{r}} \phi}$ in the hopping amplitude introduces magnetic flux $\pm\phi$ per plaquette for both spins. We will focus on the attractive case $-U < 0$ with flux $\phi = 1/3$, and on half and one third filling, while models with repulsive interactions and even denominators of ϕ have been studied in Refs. [32, 33]. In our case, the magnetic flux enlarges the unit cell threefold and there are three energy bands, as shown in Fig. 1(a-b). Since the hopping terms only connect different sublattices, the spectrum preserves particle hole symmetry. At half-filling the noninteracting system is a metal with

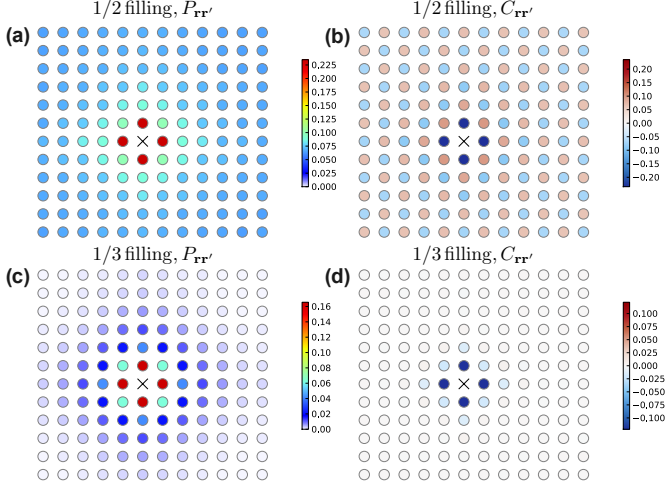


Figure 2: Superconducting and density correlation functions at $U/t = 4$. The \times symbol denotes the site \mathbf{r} relative to which correlations are shown. (a) and (b) show results for the half-filled system, while (c) and (d) for the one-third-filled system.

a nested Fermi surface. A mean field treatment of the interactions shows an instability towards s -wave pairing for infinitesimally small attraction (see Fig. 1(c)). On the other hand, the noninteracting system at $1/3$ filling is a topological insulator, and mean field theory predicts a finite critical interaction strength $U/t = 2.95$ for a transition from a correlated quantum spin Hall insulator to a BCS state, because of a vanishing density of states at Fermi level (see Fig. 1(b)).

Simulation method – We have simulated isotropic square lattices with linear size L up to 24 using an auxiliary field projective QMC algorithm [34], in which we calculate the ground state expectation values of observables \hat{O} as

$$\langle \hat{O} \rangle = \frac{\langle \Psi_T | e^{-\Theta \hat{H}/2} \hat{O} e^{-\Theta \hat{H}/2} | \Psi_T \rangle}{\langle \Psi_T | e^{-\Theta \hat{H}} | \Psi_T \rangle}. \quad (2)$$

Using a trial wave function $|\Psi_T\rangle$ with non-vanishing overlap with the ground state, Eq. (2) approaches the ground state expectation value in the large Θ limit. We use the ground state of the noninteracting Hamiltonian \hat{K} as trial state $|\Psi_T\rangle$ and $\Theta t = 50$ [59]. We break the projection into small steps and use the second-order Trotter-Suzuki decomposition $e^{-\Delta\tau \hat{H}} = e^{-\Delta\tau \hat{K}/2} e^{-\Delta\tau \hat{V}} e^{-\Delta\tau \hat{K}/2} + O(\Delta\tau^3)$ for each time step, where $\Delta\tau t = 0.05$. The interacting term $e^{-\Delta\tau \hat{V}}$ is decomposed using the Hubbard-Stratonovich transformations

$$\begin{aligned} e^{\Delta\tau U(\hat{n}_{\mathbf{r}\uparrow} - \frac{1}{2})(\hat{n}_{\mathbf{r}\downarrow} - \frac{1}{2})} &= \frac{e^{-\Delta\tau U/4}}{2} \sum_{s=\pm 1} e^{\alpha s(\hat{n}_{\mathbf{r}\uparrow} + \hat{n}_{\mathbf{r}\downarrow} - 1)} (3) \\ &= \frac{e^{\Delta\tau U/4}}{2} \sum_{s=\pm 1} e^{i\gamma s(\hat{n}_{\mathbf{r}\uparrow} - \hat{n}_{\mathbf{r}\downarrow})}, \quad (4) \end{aligned}$$

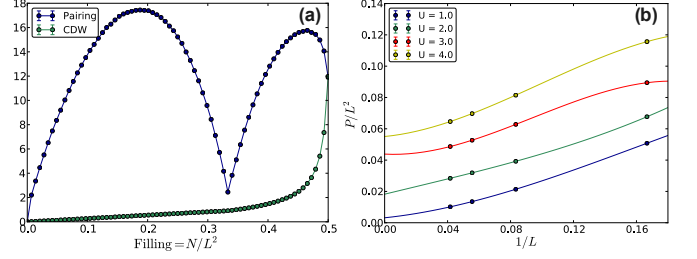


Figure 3: (a) Superconducting and CDW structure factors versus band filling in a $L = 12$ lattice with $U/t = 4$. (b) The superconducting structure factor versus $1/L$ for various interaction strengths at half-filling. The CDW structure factors are identical at half-filling due to a symmetry that is discussed in the text.

with $\cosh(\alpha) = e^{\Delta\tau U/2}$ and $\cos(\gamma) = e^{-\Delta\tau U/2}$. Both decompositions Eq. (3-4) respect the time-reversal symmetry and do not introduce sign problem in the Monte Carlo simulation. We use the decomposition Eq. (3) for the one-third filled and Eq. (4) for the half-filled system.

Correlations – We first show the superconducting pair and the density correlation functions

$$\begin{aligned} P_{\mathbf{r}\mathbf{r}'} &= \langle \hat{\Delta}_{\mathbf{r}}^\dagger \hat{\Delta}_{\mathbf{r}'} + \hat{\Delta}_{\mathbf{r}} \hat{\Delta}_{\mathbf{r}'}^\dagger \rangle, \\ C_{\mathbf{r}\mathbf{r}'} &= \langle \hat{n}_{\mathbf{r}} \hat{n}_{\mathbf{r}'} \rangle - \langle \hat{n}_{\mathbf{r}} \rangle \langle \hat{n}_{\mathbf{r}'} \rangle, \end{aligned} \quad (5)$$

in Fig. 2, where $\hat{\Delta}_{\mathbf{r}}^\dagger = \hat{c}_{\mathbf{r}\uparrow}^\dagger \hat{c}_{\mathbf{r}\downarrow}^\dagger$ and $\hat{n}_{\mathbf{r}} = \hat{n}_{\mathbf{r}\uparrow} + \hat{n}_{\mathbf{r}\downarrow}$. At $U/t = 4$ both superconducting and density correlations at half-filling extend to the farthest lattice site (in right corner), as shown in Fig. 2(a) and (b). Although the four-fold rotational symmetry of the square lattice is broken by the choice of Landau gauge in Eq. (1), it is restored in the correlation functions. The density correlation shows a staggered pattern, indicating the tendency towards forming checkerboard charge-density-wave (CDW) order. Figure 2(c) and (d) shows that at $1/3$ filling both the superconducting and CDW correlations are suppressed. In particular, the density correlation decays very rapidly. This suggests that mean-field theory overestimates the extent of the ordered phase.

To better describe the interplay between the superconducting and CDW instabilities, we calculate their respective structure factors,

$$P = \frac{1}{L^2} \sum_{\mathbf{r}, \mathbf{r}'} P_{\mathbf{r}\mathbf{r}'}, \quad (6)$$

$$C = \frac{1}{L^2} \sum_{\mathbf{r}, \mathbf{r}'} e^{-i\mathbf{Q}(\mathbf{r}-\mathbf{r}')} C_{\mathbf{r}\mathbf{r}'}, \quad (7)$$

where $\mathbf{Q} = (\pi, \pi)$. Figure. 3(a) shows the superconducting and CDW structure factor versus fillings at $U/t = 4$. The results are symmetric around half-filling because of the particle-hole symmetry of the model. The CDW

structure factor drops rapidly away from half-filling, indicating suppress of CDW order away from commensuration filling. The superconducting structure factor shows nonmonotonic behavior with filling factor. The variation is a reminiscent of the shape of the density of states (Fig.1) and is large when the phase is metallic. There is a pronounced minimum at $1/3$ filling when the lowest band is fully filled, showing that a band insulating state strongly disfavors forming of off-diagonal long range order.

At half-filling, the superconducting structure factor shows a dip and becomes equal to the CDW structure factor due to an $SU(2)$ symmetry. To reveal this symmetry we perform a particle hole transformation for the spin-down component $\hat{c}_{r\downarrow} \rightarrow e^{-i\mathbf{Q}r} \hat{c}_{r\downarrow}^\dagger$. This transformation reverses both the sign of interaction U and the magnetic flux ϕ of spin down particles. The resulting repulsive model has same magnetic flux for both spin components and is manifestly $SU(2)$ symmetric [60], explaining why superconducting and pair correlations are identical. The model is in a supersolid phase like the attractive Hubbard model at half filling [35]. The reason for this degeneracy is also transparent in the strong coupling limit, where the attractive interaction binds two fermions with opposite spin into (spinless) hard core bosons, which are inert to magnetic flux. The resulting model lies exactly at the Heisenberg point [36] and shows degenerate CDW and superfluidity instabilities.

Determining the transition – Figure 3(b) shows an extrapolation of P/L^2 at half filling (equals to C/L^2) using a third order polynomial in $1/L$. The extrapolated value gives the square of the pairing order parameter [37, 38]. Our results show that at half filling the system is already ordered at weak coupling $U/t = 1$, in agreement with the mean-field results.

However, as we have shown before, mean-field theory erroneously predicts a superconducting state at $U/t = 4$ and one third filling [61]. Figure. 4(a) shows the superconducting structure factor for various interaction strengths at $1/3$ filling. Extrapolation indicates that the transition to a superconducting state happens at $U/t \gtrsim 5.4$, a substantially larger value than the mean-field prediction $U/t = 2.95$ (Fig.1(c)). Since the time-reversal symmetry is conserved, there is no vortex lattice structure in the BCS state compare to the model studied in Ref. [39]. Again, this agrees with the fact that the hard core bosons in the strong interaction limit are inert to magnetic field.

An alternative determination of the critical interaction strength for the QSH to BCS is based on the charge gap, which can be calculated as

$$\Delta_c = \frac{E_{L^2/3+1} + E_{L^2/3-1} - 2E_{L^2/3}}{2}, \quad (8)$$

where E_N is the ground state energy of $N_\uparrow = N_\downarrow = N$ particles. Δ_c is the energy cost of adding a pair of

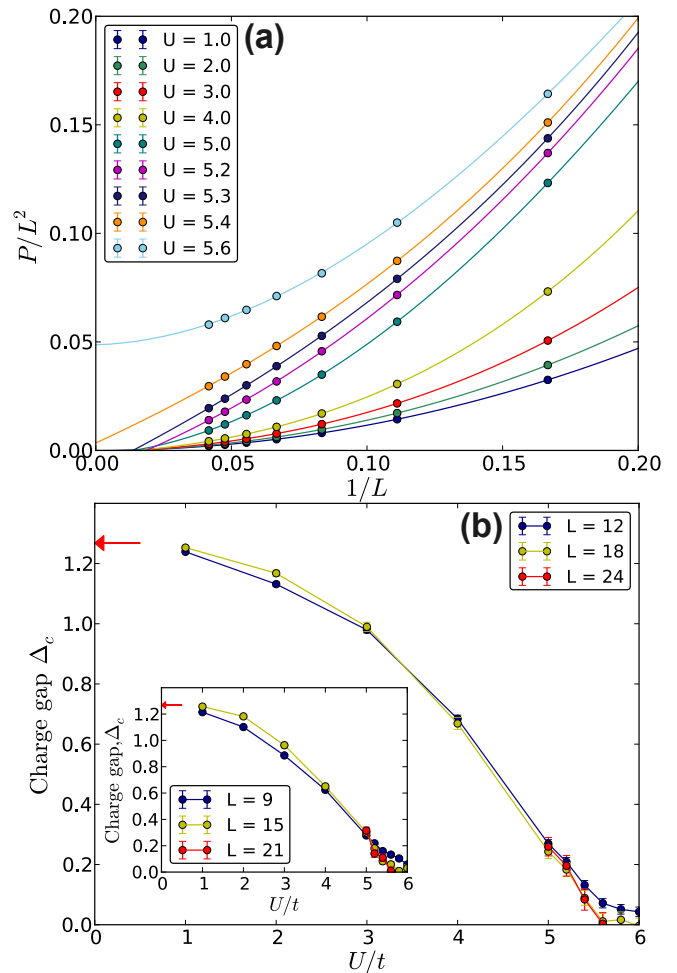


Figure 4: (a) The superconducting structure factor of a $1/3$ -filled system. Solid lines are fits with cubic function of $1/L$. (b) The charge gap Δ_c versus interaction strength U for systems with periodic boundary conditions. The inset shows the charge gap in systems with anti-periodic boundary conditions. The red arrow indicates the band gap of the noninteracting system.

fermions to the system. In the noninteracting limit it equals to the minimal band gap $1.268t$, realized at the momenta $(\pm\frac{\pi}{3}, \frac{\pi}{3})$ and $(\pi, \frac{\pi}{3})$ in the Brillouin zone (see. Fig. 1(a)). We choose boundary conditions of finite size clusters carefully to ensure that these momenta exist: we use periodic boundary condition for $L = 6, 12, 18, 24$ and anti-periodic boundary condition for $L = 3, 9, 15, 21$. Figure 4(b) shows the charge gap versus U for various system sizes. It decreases from the noninteracting value as the attractive interaction increases, and becomes zero at the quantum phase transition to the superconducting phase. We find that this happens at $U/t = 5.6$ for the largest system we have calculated, consistent with transition point $U \gtrsim 5.4$ estimated from the superconducting correlations.

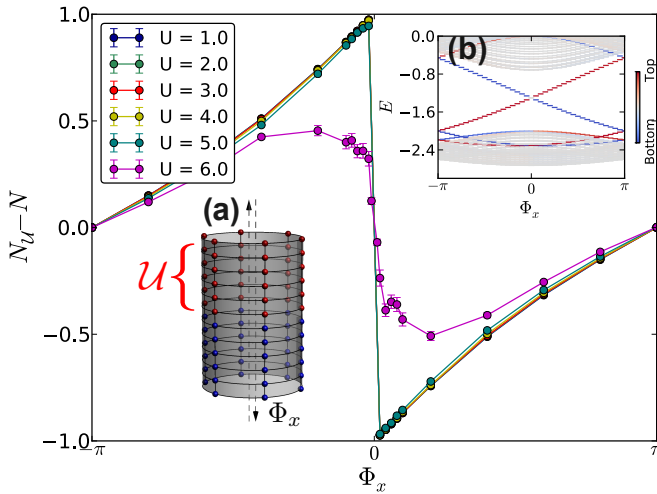


Figure 5: Total particle number in the upper-half of a cylinder (Eq.(9)) versus flux Φ_x for various interaction strengths. Inset (a) illustrates a flux Φ_x (opposite for spin \uparrow and \downarrow) threaded through the cylinder, which pumps particles vertically in the QSH phase. Sites in the upper half of the cylinder are shown in red and their occupation numbers sum to N_U . Inset (b) shows single particle energy levels versus the threaded flux Φ_x in a cylindrical noninteracting system. Color indicates the center-of-mass of single particle wave functions, with red (blue) being closer to the upper (lower) edge.

Topological nature of the transition – The QSH state is characterized by a nontrivial topological \mathbb{Z}_2 index [40], and we expect the system to remain in this phase until the transition point. Several approaches have been proposed to characterize interacting topological insulators [41–43]. However they either require approximations [24] or miss the interaction induced phase transition [44–47].

To directly reveal the topological nature of the QSH-BCS transition, we thread a flux through a cylinder [29] and probe the topological charge pumping effect [30, 31, 48]. Figure 5(a) shows a flux $+\Phi_x$ ($-\Phi_x$) for spin up (down) particles threaded through a cylinder, which amounts to introducing spin-dependent twisted boundary conditions [49, 50]. Since spin up and down particles feel opposite magnetic fluxes (both Φ_x and ϕ), time reversal symmetry is preserved and there is no sign problem in the QMC simulations. When Φ_x changes from $-\pi$ to π both spin up and down particles are pumped along the same vertical direction [62]. The total pumped charge is proportional to the spin Chern number [50], which is the difference of the Chern number for spin up and down particles and directly probes the quantum spin Hall effect.

To get a better understanding of the topological pumping effect, inset (b) of Fig. 5 shows the single particle energy spectrum versus Φ_x on a cylinder with a circumference of six sites. Color indicates the center-of-mass position of each eigenstate, with red (blue) color being

closer to the upper (lower) edge. There are two edge states corresponding to the cylinder’s top and bottom edge, which cross at $\Phi_x = 0$. In the $1/3$ filled system, the Fermi level lies exactly at this crossing point and the density distribution is symmetric in the absence of a flux Φ_x . Inserting an infinitesimal flux moves the particles towards to one of the edges and introduces a polarization along the cylinder. Further increase of Φ_x pumps the particle vertically, thereby changing the polarization. The total change of polarization upon inserting a 2π flux gives the spin Chern number. This topological pumping effect is robust against interactions and can be used to distinguish the correlated \mathbb{Z}_2 topological insulators and a topological trivial superfluid state.

To quantify the topological pumping effect we calculate the total particle number in the upper part of the cylinder (see Fig.5(a))

$$N_U = \sum_{\mathbf{r} \in U} (n_{\mathbf{r}\uparrow} + n_{\mathbf{r}\downarrow}). \quad (9)$$

The total number of particles pumped to the upper half of the cylinder is $\int_{-\pi}^{\pi} \frac{dN_U}{d\Phi_x} d\Phi_x$. Because N_U is periodic with Φ_x , there must be discontinuities in N_U to account for the finite shift. The size of the discontinuity is again equal to the spin-Chern number, and strong evidence for the presence of a QSH state in the interacting system. Figure 5 shows $N_U - N$ versus Φ_x for various interaction strengths [63]. Inside the QSH state ($U/t = 1, 2, 3, 4, 5$), the curves are almost identical and they all show an overall shift of two, which is the spin Chern number of the QSH state. The discontinuity at $\Phi_x = 0$ is a characteristic behavior of the topological nontrivial state. After the transition to the BCS state ($U/t = 6$) the discontinuity disappears and the pumped charge is zero. These results provide a direct topological signature of the QSH-BCS transition. Being related but different from the π -flux insertion method [51, 52] used in Ref. [20], the charge pumping approach directly probes the topological response of a QSH state and can be easily generalized to systems with spin-flip terms [48, 50, 52].

Outlook – Our work opens up a number of exciting possibilities for studying strongly correlated topological phases using numerical exact quantum Monte Carlo methods. For example, it will be interesting to further study the correlation effect in a Hofstadter model with arbitrary fluxes, where the occupied band has higher Chern number or even a fractal energy spectrum. Topological charge pumping probe can also be used to identify the fractional topological phases [53, 54]. A detailed study of edge physics in conjunction with the topological pumping probe will also be of interest. Experimentally, our results are directly relevant to current studies of Hofstadter model in cold atom systems [7, 8, 55]. Along this line, we leave a detailed study of the finite temperature phase diagram and inhomogeneity effects for future study.

Acknowledgments – We thank J. Gukelberger, M. Dolfi and A. Soluyanov for discussion and support. Simulations were performed on the Mönch cluster of Platform for Advanced Scientific Computing (PASC), the Brutus cluster at ETH Zurich, and the “Monte Rosa” Cray XE6 at the Swiss National Supercomputing Centre (CSCS). H.H.H. acknowledges the computational support from the Center for Scientific Computing at the CNSI and MRL through NSF MRSEC (DMR-1121053) and NSF CNS-0960316. We have used ALPS libraries [56] for Monte Carlo simulations and data analysis. This work was supported by ERC grant SIMCOFE.

-
- [1] D. R. Hofstadter, *Phys. Rev. B* **14**, 2239 (1976).
 - [2] K. v. Klitzing, G. Dorda, and M. Pepper, *Phys. Rev. Lett.* **45**, 494 (1980).
 - [3] D. Osadchy and J. E. Avron, *J. Math. Phys.* **42**, 5665 (2001).
 - [4] C. R. Dean, L. Wang, P. Maher, C. Forsythe, F. Ghahari, Y. Gao, J. Katoch, M. Ishigami, P. Moon, M. Koshino, T. Taniguchi, K. Watanabe, K. L. Shepard, J. Hone, and P. Kim, *Nature* **497**, 598 (2013).
 - [5] B. Hunt, J. D. Sanchez-Yamagishi, A. F. Young, M. Yankowitz, B. J. LeRoy, K. Watanabe, T. Taniguchi, P. Moon, M. Koshino, P. Jarillo-Herrero, and R. C. Ashoori, *Science* **340**, 1427 (2013).
 - [6] L. A. Ponomarenko, R. V. Gorbachev, G. L. Yu, D. C. Elias, R. Jalil, A. A. Patel, A. Mishchenko, A. S. Mayorov, C. R. Woods, J. R. Wallbank, M. Mucha-Kruczynski, B. A. Piot, M. Potemski, I. V. Grigorieva, K. S. Novoselov, F. Guinea, V. I. Fal’ko, and A. K. Geim, *Nature* **497**, 594 (2013).
 - [7] M. Aidelsburger, M. Atala, M. Lohse, J. T. Barreiro, B. Paredes, and I. Bloch, *Phys. Rev. Lett.* **111**, 185301 (2013).
 - [8] H. Miyake, G. A. Siviloglou, C. J. Kennedy, W. C. Burton, and W. Ketterle, *Phys. Rev. Lett.* **111**, 185302 (2013).
 - [9] C. J. Kennedy, G. A. Siviloglou, H. Miyake, W. C. Burton, and W. Ketterle, *Phys. Rev. Lett.* **111**, 225301 (2013).
 - [10] C. L. Kane and E. J. Mele, *Phys. Rev. Lett.* **95**, 226801 (2005).
 - [11] B. A. Bernevig, T. L. Hughes, and S. C. Zhang, *Science* **314**, 1757 (2006).
 - [12] M. Z. Hasan and C. L. Kane, *Rev. Mod. Phys.* **82**, 3045 (2010).
 - [13] X.-L. Qi and S.-C. Zhang, *Rev. Mod. Phys.* **83**, 1057 (2011).
 - [14] M. König, S. Wiedmann, C. Brüne, A. Roth, H. Buhmann, L. W. Molenkamp, X. L. Qi, and S. C. Zhang, *Science* **318**, 766 (2007).
 - [15] S. Rachel and K. Le Hur, *Phys. Rev. B* **82**, 075106 (2010).
 - [16] M. Hohenadler, T. C. Lang, and F. F. Assaad, *Phys. Rev. Lett.* **106**, 100403 (2011).
 - [17] M. Hohenadler, Z. Y. Meng, T. C. Lang, S. Wessel, A. Muramatsu, and F. F. Assaad, *Phys. Rev. B* **85**, 115132 (2012).
 - [18] S.-L. Yu, X. C. Xie, and J.-X. Li, *Phys. Rev. Lett.* **107**, 010401 (2011).
 - [19] D. Zheng, G.-M. Zhang, and C. Wu, *Phys. Rev. B* **84**, 205121 (2011).
 - [20] F. F. Assaad, M. Bercx, and M. Hohenadler, *Phys. Rev. X* **3**, 011015 (2013).
 - [21] C. N. Varney, K. Sun, M. Rigol, and V. Galitski, *Phys. Rev. B* **82**, 115125 (2010).
 - [22] C. N. Varney, K. Sun, M. Rigol, and V. Galitski, *Phys. Rev. B* **84**, 241105 (2011).
 - [23] L. Wang, H. Shi, S. Zhang, X. Wang, X. Dai, and X. C. Xie, *arXiv cond-mat.str-el* (2010).
 - [24] L. Wang, X. Dai, and X. C. Xie, *EPL* **98**, 57001 (2012).
 - [25] T. Yoshida, R. Peters, S. Fujimoto, and N. Kawakami, *Phys. Rev. B* **87**, 085134 (2013).
 - [26] M. Hohenadler and F. F. Assaad, *J. Phys.: Condens. Matter* **25**, 143201 (2013).
 - [27] M. Troyer and U.-J. Wiese, *Phys. Rev. Lett.* **94**, 170201 (2005).
 - [28] C. Wu and S.-C. Zhang, *Phys. Rev. B* **71**, 155115 (2005).
 - [29] R. B. Laughlin, *Phys. Rev. B* **23**, 5632 (1981).
 - [30] D. J. Thouless, *Phys. Rev. B* **27**, 6083 (1983).
 - [31] Q. Niu and D. J. Thouless, *Journal of Physics A: Mathematical and General* **17**, 2453 (1984).
 - [32] D. Cocks, P. P. Orth, S. Rachel, M. Buchhold, K. Le Hur, and W. Hofstetter, *Phys. Rev. Lett.* **109**, 205303 (2012).
 - [33] C.-C. Chang and R. T. Scalettar, *Phys. Rev. Lett.* **109**, 026404 (2012).
 - [34] F. F. Assaad and H. G. Evertz, *Computational Many Particle Physics, Lecture Notes in Physics* **739**, 277 (2008).
 - [35] J. E. Hirsch, *Phys. Rev. B* **31**, 4403 (1985).
 - [36] G. Schmid, S. Todo, M. Troyer, and A. Dorneich, *Phys. Rev. Lett.* **88**, 167208 (2002).
 - [37] D. A. Huse, *Phys. Rev. B* **37**, 2380 (1988).
 - [38] R. T. Scalettar, E. Y. Loh, J. E. Gubernatis, A. Moreo, S. R. White, D. J. Scalapino, R. L. Sugar, and E. Dagotto, *Phys. Rev. Lett.* **62**, 1407 (1989).
 - [39] H. Zhai, R. O. Umucalilar, and M. O. Oktel, *Phys. Rev. Lett.* **104**, 145301 (2010).
 - [40] C. L. Kane and E. J. Mele, *Phys. Rev. Lett.* **95**, 146802 (2005).
 - [41] L. Wang, X. Dai, and X. C. Xie, *Phys. Rev. B* **84**, 205116 (2011).
 - [42] L. Wang, H. Jiang, X. Dai, and X. C. Xie, *Phys. Rev. B* **85**, 235135 (2012).
 - [43] Z. Wang and S.-C. Zhang, *Phys. Rev. X* **2**, 031008 (2012).
 - [44] H.-H. Hung, L. Wang, Z.-C. Gu, and G. A. Fiete, *Phys. Rev. B* **87**, 121113 (2013).
 - [45] T. C. Lang, A. M. Essin, V. Gurarie, and S. Wessel, *Phys. Rev. B* **87**, 205101 (2013).
 - [46] H.-H. Hung, V. Chua, L. Wang, and G. A. Fiete, *arXiv cond-mat.str-el* (2013).
 - [47] Z. Y. Meng, H.-H. Hung, and T. C. Lang, *Mod. Phys. Lett. B*, 1430001 (2013).
 - [48] A. Alexandradinata, T. L. Hughes, and B. A. Bernevig, *Phys. Rev. B* **84**, 195103 (2011).
 - [49] X.-L. Qi, Y.-S. Wu, and S.-C. Zhang, *Phys. Rev. B* **74**, 045125 (2006).
 - [50] D. Sheng, Z. Weng, L. Sheng, and F. Haldane, *Phys. Rev. Lett.* **97**, 036808 (2006).
 - [51] Y. Ran, A. Vishwanath, and D.-H. Lee, *Phys. Rev. Lett.* **101**, 086801 (2008).
 - [52] X.-L. Qi and S.-C. Zhang, *Phys. Rev. Lett.* **101**, 086802 (2008).

- [53] K. Yang and H. Zhai, *Phys. Rev. Lett.* **100**, 030404 (2008).
- [54] H. Chen and K. Yang, *Phys. Rev. B* **85**, 195113 (2012).
- [55] C. Chin and E. J. Mueller, *Physics* **6**, 118 (2013).
- [56] B. Bauer et al, *J. Stat. Mech.: Theor. Exp.* **2011**, P05001 (2011).
- [57] F. Assaad, *Phys. Rev. B* **65**, 115104 (2002).
- [58] L. Fu and C. Kane, *Phys. Rev. B* **74**, 195312 (2006).
- [59] At half-filling to avoid open shell effect we add one additional flux quantum to the system [57] when generating $|\Psi_T\rangle$.
- [60] This is different from the Kane-Mele-Hubbard model [16] and the model studied in [32], where SU(2) spin symmetry is broken explicitly.
- [61] The CDW correlation is substantially suppressed at this filling and does not compete with superconductivity.
- [62] This is different from the spin pump studied in Ref. [58] where up and down particles move in opposite directions.
- [63] Because of the presence of low lying excited states close to $\Phi_x = 0$, we use much larger projection parameter $\Theta t = 200$ to obtain a converged ground state density.